APL Materials

A new era in ferroelectrics

Cite as: APL Mater. **8**, 120902 (2020); https://doi.org/10.1063/5.0034914
Submitted: 28 October 2020 . Accepted: 10 November 2020 . Published Online: 04 December 2020

S. Das, Z. Hong, M. McCarter, P. Shafer, Yu-Tsun Shao, D. A. Muller, L. W. Martin, and R. Ramesh

A new era in ferroelectrics

Cite as: APL Mater. 8, 120902 (2020); doi: 10.1063/5.0034914
Submitted: 28 October 2020 • Accepted: 10 November 2020 •
Published Online: 4 December 2020

S. Das,[1,2,a] Z. Hong,[3] M. McCarter,[2] P. Shafer,[4] Yu-Tsun Shao,[5] D. A. Muller,[5,6] L. W. Martin,[1,7] and R. Ramesh[1,2,7,a]

AFFILIATIONS

[1]Department of Materials Science and Engineering, University of California, Berkeley, California 94720, USA
[2]Department of Physics, University of California, Berkeley, California 94720, USA
[3]Department of Materials Science and Engineering, Zheijian University, Hangzhou, China
[4]Advanced Light Source, Lawrence Berkeley National Laboratory, Berkeley, California 94720, USA
[5]School of Applied and Engineering Physics, Cornell University, Ithaca, New York 14853, USA
[6]Kavli Institute at Cornell for Nanoscale Science, Ithaca, New York 14853, USA
[7]Materials Sciences Division, Lawrence Berkeley National Laboratory, Berkeley, California 94720, USA

Note: This paper is part of the Special Topic on 100 Years of Ferroelectricity—A Celebration.
[a]**Authors to whom correspondence should be addressed:** sujitdas@berkeley.edu and rramesh@berkeley.edu

ABSTRACT

Topological structures in ferroic materials have drawn great interest in recent years due to the richness of the underlying physics and the potential for applications in next generation electronics. Recent advances in atomically precise thin-film materials synthesis and characterization of structural/physical phenomena at unprecedented length/energy/time scales have enabled us to study exotic phases and their associated physics [Rößler *et al.*, Nature **442**, 797 (2006); S. Das, Nature **568**, 368 (2019); Yadav *et al.*, Nature **530**, 198 (2016); and Stoica *et al.*, Nat. Mater. **18**, 377 (2019)].[14] It is appropriate that, in the second century of ferroelectrics, some dramatic discoveries are propelling the field into directions heretofore unimaginable. In this review, we explore the recent progress in ferroelectric-oxide superlattices in which researchers can control structure and physical properties through the application of epitaxial strain, layer thickness, temperature, electric field, etc. We provide a discussion of exotic topological structures (e.g., closure domains, vortices, polar skyrmions, and other exotic phases) and associated functionalities in ferroelectric/paraelectric superlattices. We conclude with a brief overview of and prospects for how the field may evolve in the coming years.

INTRODUCTION

In the hundred years since the original discovery of ferroelectricity in Rochelle salt,[5] numerous significant discoveries and technological manifestations of these materials have been demonstrated.[6] While it is essentially impossible to cover all of these discoveries in a single review, we attempt to put into perspective some striking new discoveries within the family of well-known perovskite ferroelectrics, driven by the confluence of three scientific advances in the field. The first is the ability of materials synthesis approaches to control and tailor artificially designed materials at the atomic scale, as exemplified by the creation of epitaxial superlattices,[7] the second is the dramatic advancements in *ab initio* and mesoscale phase-field computational approaches,[8,9] and the third is the emergence of a host of probes using x-rays, electrons, and neutrons and near field techniques that are now routinely enabling us to study physical phenomena at the atomic scale at unprecedented length/energy/time scales. In parallel, there has been a revolution developing that is exploring the possibility of using ferroelectrics as a key element in beyond Moore's law electronics, serving the dual role of a memory element and enabling logic operations.[10] Another key manifestation of ferroelectrics is in the form of magnetoelectric multiferroics, exemplified by the ferroelectric $BiFeO_3$. While we urge the interested reader to explore recent reviews on this subject,[11] this review is focused on emergent topologies in ferroelectrics. These recent discoveries

have renormalized our thinking about the fundamental nature of ferroelectricity.

The classical thinking (i.e., ferroelectrics vs ferromagnets) had been that ferroelectrics represent the extreme case where the dipolar interaction is of a lower energy scale than the anisotropy (which comes about directly due to the strong dipole–lattice coupling) that manifests as a strong lattice distortion below the transition temperature (e.g., the prototypical ferroelectric $PbTiO_3$ has a strong tetragonal distortion of about 5%). In contrast, ferromagnets are exemplified by a much stronger exchange energy than the anisotropy energy (except for ferromagnets which contain rare earth ions with inherently large spin–orbit coupling). As an immediate manifestation, the domain-wall width (which is directly related to the tradeoff between these two energies) is small in ferroelectrics (a few unit cells wide) since anisotropy dominates. In contrast, domain-wall widths in classical ferromagnets (e.g., iron and cobalt) are much larger than the unit-cell dimensions since exchange dominates. As a direct consequence of the strong role played by anisotropy energy in ferroelectrics, rotations of the dipoles away from the crystallographic easy axes (e.g., the [001] in tetragonal $PbTiO_3$) have always been thought to be challenging. Work in the past decade (particularly in the last five years), however, has shown that this is likely not the case.[2,3] When appropriate boundary conditions[4] are imposed onto the ferroelectric crystal, it is forced to take up dipolar arrangements that exhibit exotic topologies that are typically not favored in the bulk. This forms the backbone for our discussion in this review.

Topology is a branch of mathematics that studies the properties of geometric objects that are preserved under continuous deformations – such as under contraction, expansion, rotation, etc.[12] In recent years, topological states, for example, spin/dipolar textures, have become an intense topic of study in condensed-matter physics and materials science,[1] and the concept of topology[13,14] has been woven into condensed-matter physics.[15,16] Topology can arise in either real-space arrangements of the order parameter (i.e., dipole moment, spins, etc.) or in reciprocal space arising from the topology of the band structure, leading to topological insulators, semimetals, and superconductors.[17] Focusing on real-space topologies, textures such vortices and skyrmions of ferroic order have attracted attention in the past decade due to their exotic nature and the consequent diversity of interesting physics and properties that hold promise for future technologies.[18–20] The formation of domains in ferroic materials such as ferroelastics, ferromagnets, or ferroelectrics is due to the thermodynamic driving force to reduce the depolarization/demagnetization/strain fields that occur at surfaces or interfaces. Regions of the uniform order parameter are separated by domain walls, which can be thought of as a two-dimensional (2D) topological defect. The three archetypes of domain walls are classified by either their axis of rigid rotation (Néel and Bloch type) or the scaling of the moment across the wall (Ising type).[21–23] Despite their chemical and phase homogeneity, even basic domain walls approximating these archetypes will exhibit emergent properties due to the broken symmetry and strong spin, lattice, and charge coupling of the respective ferroic order.[24–28] Formation of complex topologies, however, has, until recently, been the purview of ferromagnetic materials whose relative isotropy, rigid spin moments, and exchange energy produce rotational Néel and Bloch walls as well as complex textures such as helices, vortices, and skyrmions.[29] Furthermore, in ferromagnets, the formation of spin textures requires symmetry breaking either in the form of an interface breaking inversion symmetry or in the bulk through the anti-symmetric Dzyalozhinski–Moriya coupling. Three-dimensional (3D) topological defects with different geometric shapes can appear in ferroic materials under specific conditions. Typical topological defects include vortices, skyrmions, merons, etc. (Fig. 1).[4,30–34] Although these topological defects may decay over time in the bulk, they are surprisingly stable in nanoscale systems. At the same time, they are responsive to external fields (mechanical, thermal, electric, and magnetic), which may lead to exotic physics such as chirality reversal,[35] ratchet effects,[36] negative electrocaloric effects,[37] negative capacitance effects,[38] etc.

Kittel's work (dating to 1949)[39] in magnetic materials outlined the formation of different magnetization patterns depending on the competition of various energies associated with the exchange and crystallographic anisotropy as well as electrostatic/magnetostatic energy arising from depolarization/demagnetization fields.[40] A flux-closure-like domain is predicted when anisotropy energy dominates, whereas, a vortex-like structure is developed when exchange interactions between adjacent magnetic moments dominate over anisotropy. It is easy to find such arrangements of magnetic dipoles when the material is reduced to small sizes, and this has led to experimental observations of flux-closure domains and vortices.[12,41–47] More complex topological structures can be developed in ferroic materials – i.e., those with a spontaneous reversible ordering, for example, magnetic skyrmions with swirling arrangements of magnetic dipoles, as described by Mermin [Fig. 1(e)].[12,45,48,49] Magnetic flux-closure domains were first observed in permalloy plates and disks.[50] When permalloy films are reduced to smaller sizes to form circular disks (of ~1 μm diameter), the magnetic moments become arranged into continuous circular loops, forming vortex structures instead of flux-closure domains.[39] Complex magnetic topological patterns like a periodic array of magnetic skyrmions have also been recently observed in $(Fe_{0.5}Co_{0.5})Si$.[47] Finally, one key attribute that underlies the formation of such spin textures is the existence of inversion symmetry breaking, for example, through an interfacial Rashba effect[51] or an anti-symmetric Dzyalozhinski–Moriya interaction.

It was heretofore thought that formation of such textures in ferroelectrics would be difficult, which exhibit large crystalline anisotropy (because dipole–lattice coupling is much stronger than spin–lattice coupling). However, the emergence of sophisticated computational methods[52,53] has triggered an intellectual renaissance in this field. Such theoretical studies in ferroelectric nanostructures first showed enormous potential in formation of new electric-dipole arrangements including those with a toroidal moment (which is nonzero for a curling configuration of electric dipoles) in $BaTiO_3$ and $PbZr_{0.5}Ti_{0.5}O_3$.[54,55] Ferroelectric domain walls do exhibit rotational components[56] including a pronounced Néel character in the vicinity of the domain-wall interface terminations where minimization of stray field energies leads to domain broadening[57] and formation of rotational flux-closure structures[58,59] including closed loops.[3,60] In the absence of an equivalent mechanism for a proper ferroelectric, non-collinear moments such as chiral host structures or spin–orbit interactions,[61] vortices, and "hedgehog" skyrmions are the most promising parity structures that might be obtained through these rotational–ferroelectric transitions. Experimentally, it was shown that ferroelectric flux-closure-domain topologies can

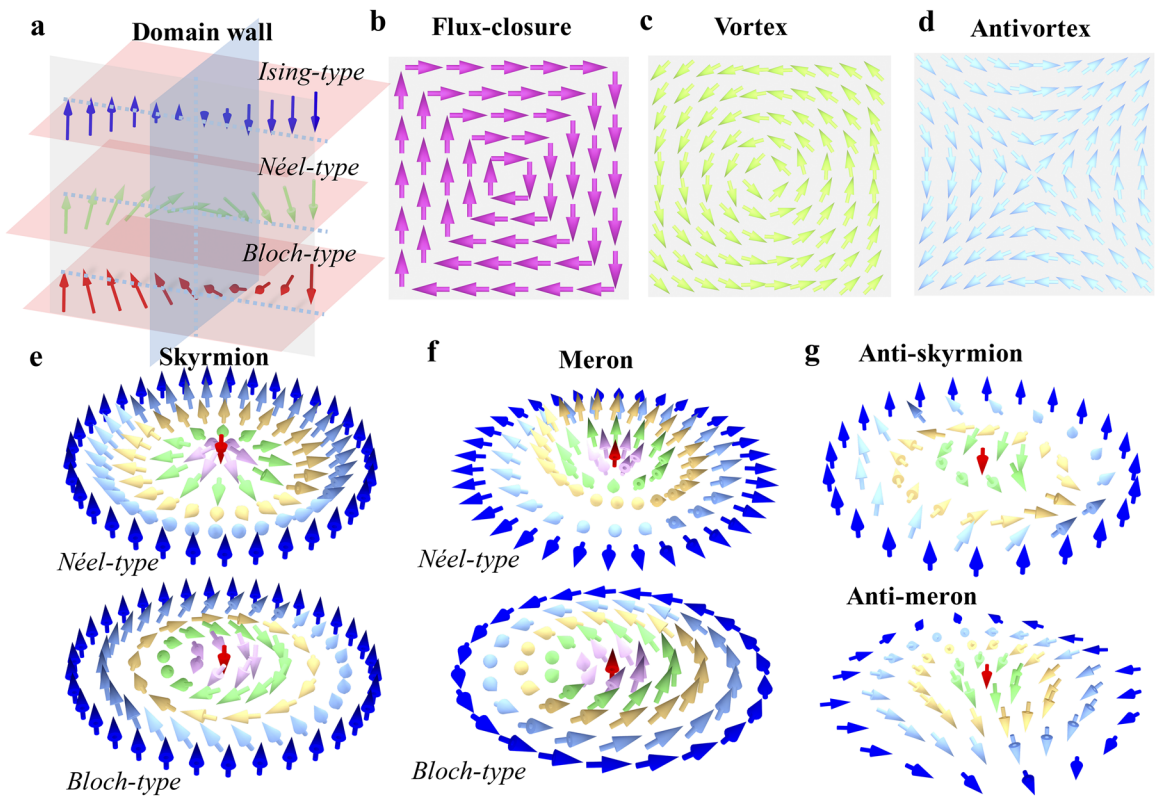

FIG. 1. Schematics of topological textures in ferroics. The arrows represent the polarization or magnetization. (a) Different types of domain walls; (b) flux-closure; (c) vortex (d) antivortex; (e) Néel-type and Bloch-type skyrmion; (f) Néel-type and Bloch-type meron; (g) anti-skyrmion and anti-meron.

emerge, similar to those in a ferromagnet, by juxtaposing the dimensionality of layer thickness, strain, and electrostatic energies.[55] Such flux-closure domain structures in ferroelectrics were first observed in $PbZr_{0.2}Ti_{0.8}O_3$ layers and later in a $PbTiO_3$ layer.[58,60] Despite this interest, the first experimental realization of continuously rotating polar topological configurations (polar vortices) and swirling polar topological configurations (polar skyrmions) in $(PbTiO_3)_n/(SrTiO_3)_n$ heterostructures was demonstrated only recently.[2,3] This required the convergence of precise materials synthesis, oxide superlattices in this case, in which thermodynamic boundary conditions are imposed on a ferroelectric phase and directly studied with state of the art material characterization tools.[3] With this as the background, this review focuses on the advances and breakthroughs over the past decade (particularly the past five years) in the growth of ferroelectric model systems and their topological structures. We focus on polar vortices, polar skyrmions, and the associated functionalities recently observed in ferroelectric epitaxial heterostructures. Finally, we conclude this review with an outlook for this burgeoning field.

Growth of $(PbTiO_3)_m/(SrTiO_3)_n$ as a model system

Bringing together advances in reflection high-energy electron diffraction (RHEED) controlled layer-by-layer growth, the similarity of in-plane lattice parameters of $PbTiO_3$ and $SrTiO_3$, and advanced microscopy techniques, superlattices are ideal model systems to study the effects of the competition between various components of the ferroelectric Hamiltonian, in a manner that is not present in the bulk form. Short-period $(PbTiO_3)_m/(SrTiO_3)_n$ interfaces also lead to the emergence of improper ferroelectricity due to antiferrodistortive/ferroelectric coupling, driven by interfacial oxygen octahedral rotations.[62–64] It has also been shown that in $(PbTiO_3)_m/(SrTiO_3)_n$ (m, $n < 9$ unit cells) superlattices, $PbTiO_3$ has a local negative dielectric constant which imbues a large overall, positive permittivity to the superlattice.[65,66] At relatively large length scales (m, $n > 20$ unit cell), these superlattices form classical flux-closure domain patterns in order to reduce the depolarization fields.[57,59] At intermediate length scales (n and $m = 10–20$ unit cells), however, theoretical studies suggested that such superlattices could potentially support the formation of exotic topological structures (vortices and skyrmions) as a result of the competition of different energies (i.e., elastic, depolarization, and gradient).[53,67–69] What this work has demonstrated is that careful control of material heterostructures and the local competition of energies can provide a potential pathway to manipulate the structural, polar, and physical nature of the mesoscale structures that emerge.[53,70–72]

On the synthesis side, the most important recognition came with the realization that having excess of lead in the target is

beneficial to the layer-by-layer growth of the $PbTiO_3$ layers in the superlattices. As a direct consequence, such a growth mode can be maintained up to even 200 nm of total thickness. One of RHEED-controlled growths of $(SrTiO_3)_6/(PbTiO_3)_6$ superlattices (Fig. 2) reveals RHEED oscillations that are present throughout the growth of the 100-nm-thick superlattice, indicating that both the $PbTiO_3$ and $SrTiO_3$ layers are grown in a layer-by-layer fashion, which, in turn, enables controlled growth of the superlattices with different period-thicknesses while achieving the same total thickness.[3] Thus, it should not be surprising that atomically sharp chemical interfaces can be observed in cross-sectional, STEM images [Fig. 2(b)], and atomic-scale high-resolution STEM (HR-STEM) confirms sharp and coherent interfaces (b). As we will discuss later, such chemically sharp interfaces (i.e., with a minimum of interfacial interdiffusion) are critical to impose other thermodynamic boundary conditions on the superlattice. With such atomically ideal superlattices on hand, one can ask the following: what are the consequences of the imposition of such electrostatic and elastic boundary conditions on the $PbTiO_3$ layer?

Polar vortices

The first surprise from HR-STEM studies came when the atomic-resolution images were analyzed using vector-mapping algorithms. In contrast to what was expected, researchers observed rotating patterns in dark-field transmission electron microscopy (DF-TEM) images [Fig. 3(a)] comprising a long-range, periodic array of intensity modulations along both the in- and out-of-the plane directions of the superlattice with a spacing of ~10 nm. At higher resolution [Fig. 3(b)], vector mapping of the atomic polar displacement ($\boldsymbol{P}_{PD}$)[44] in a cross-sectional HR-STEM image enabled researchers to measure the local non-centrosymmetry of the lattice. The vector map of these polar displacements indicates the formation of long-range arrays of clockwise (CW) and counter clockwise (CCW) vortex pairs in each $PbTiO_3$ layer. A single CW-CCW vortex pair is shown in the magnified image [Fig. 3(c)] and reveals the full density of data points (one for each atom) and the continuous rotation of the polarization state within the vortices. The lateral periodicity of this pair is ~10 nm (and scales with the superlattice periodicity). Such pairs of CW-CCW vortices have been confirmed by both second-principles calculations[8] and phase-field simulations.[73] The 3D structure of the CW-CCW array of a vortex in the $(PbTiO_3)_{10}/(SrTiO_3)_{10}$ superlattice from phase-field simulation [right, Fig. 3(d)] and the experimental HR-STEM studies where cross-sectional and planar-view DF-TEM images [left, Fig. 3(d)] can be projected onto the same 3D axes are compared. In the 3D structural model, the polarization rotation is mapped onto the front plane

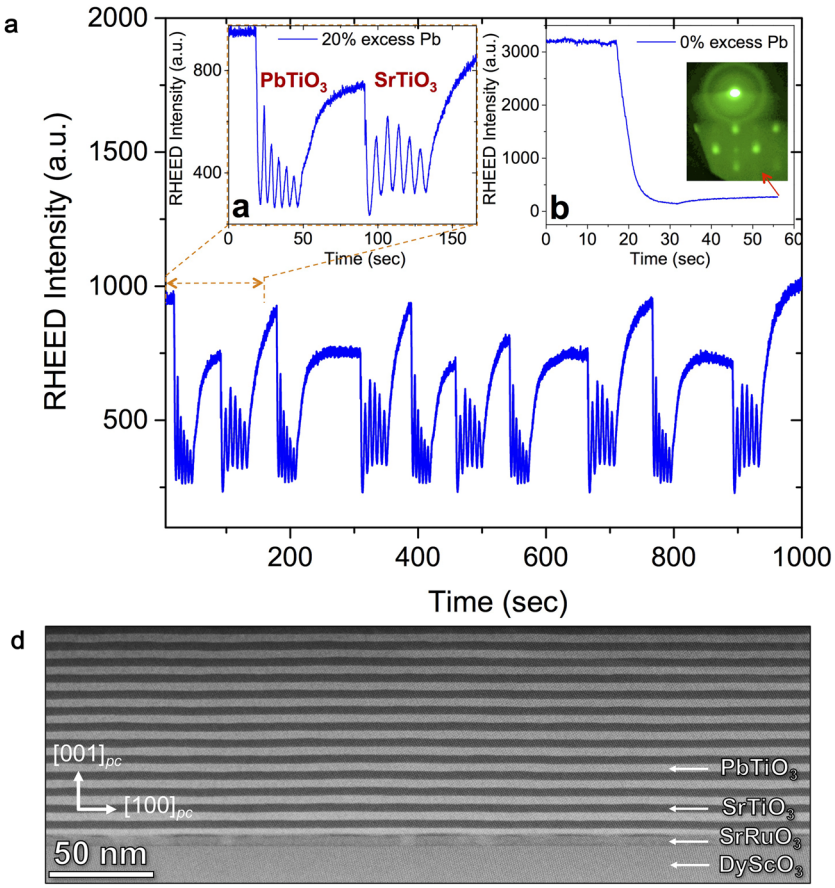

FIG. 2. RHEED-controlled growth and structural characterization of $(SrTiO_3)_6/(PbTiO_3)_6$ superlattices. (a) RHEED oscillations for five periods of the superlattice grown using a 20% excess Pb target are shown. The oscillations were present throughout the growth of the 100-nm-thick superlattice. (b) RHEED oscillations for six unit cells of $PbTiO_3$, followed by oscillations for six unit cells of $SrTiO_3$, that is, one 6 × 6 superlattice period. (c) RHEED intensity variation for growth of $PbTiO_3$ from a stoichiometric $PbTiO_3$ or 0% Pb excess target. Inset, RHEED diffraction pattern obtained at the end of growth, highlighting the rapid transition to 3D growth mode when a stoichiometric target is used. (d) Low magnification, STEM image of the cross-section of a $(SrTiO_3)_{10}/(PbTiO_3)_{10}$ superlattice reveals the layer uniformity. Reproduced with permission from Yadav *et al.*, Nature **530**, 198 (2016). Copyright 2016 Springer Nature.

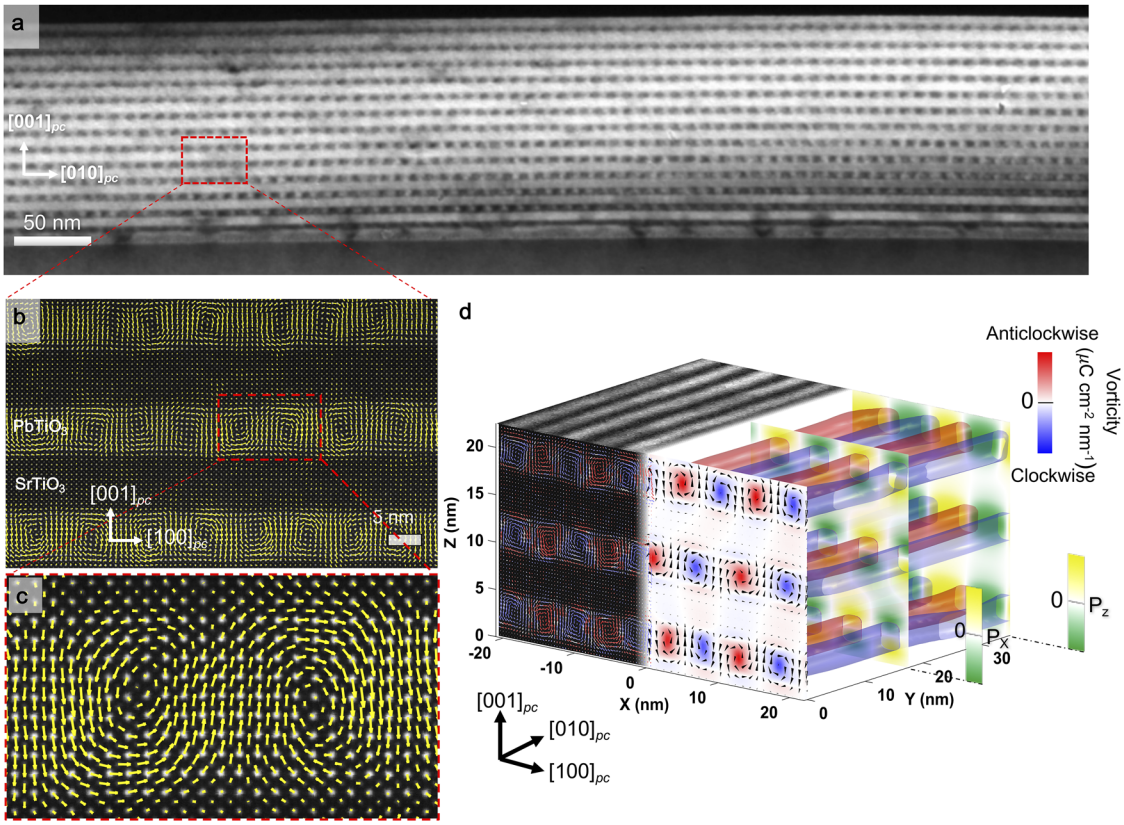

FIG. 3. Long range periodic array of vortex structures in $(SrTiO_3)_{10}/(PbTiO_3)_{10}$ superlattice on 5 nm SrRuO3 on DyScO3 (110) substrates. (a) Low magnification cross-sectional DF-TEM images of the superlattice showing long-range ordering of vortices. each light–dark contrast change is a CW-CCW vortex pair. (b) Cross-sectional HR-STEM image with Ti ion displacement vectors maps ($\boldsymbol{P}_{PD}$, indicated by yellow arrows), revealing a long range array of CW-CCW vortex pairs is present in each $PbTiO_3$ layer of the superlattice. (c) A magnified image of a single CW-CCW vortex pair. (d) Three-dimensional phase-field simulation with experimental HR-STEM studies. The array of CW-CCW vortex pairs from phase-field simulation is shown on the right. For comparison, on the left is shown a cross-sectional HR-STEM image overlaid with a polar displacement vector map and a planar-view DF-TEM image projected onto the front and top planes of the axes, respectively. Reproduced with permission from Yadav *et al.*, Nature **530**, 198 (2016). Copyright 2016 Springer Nature.

of the structure alternating CW (blue) vortices and CCW (red) vortices according to the curl of the polarization which extends along the $[010]_{pc}$ as long tubes, indicating ordered vortices. Red/blue color scales correspond to the curl of the polarization extracted from the phase-field model and the HR-STEM polar displacement map ($\boldsymbol{P}_{PD}$). The phase-field models indicate the formation of a CW-CCW array of the vortex ground state, bearing close resemblance to the experimental observations from HR-STEM studies. On the basis of both the experimental results and the phase-field simulations, one can conclude that the vortex structure results from competition between three energies: (1) elastic energy [the $PbTiO_3$ layers are under tensile strain on the $DyScO_3$ (110) substrate], (2) electrostatic energy from built-in fields (arising from the large polar discontinuity at the interfaces from $PbTiO_3$ to $SrTiO_3$ layers), and (3) gradient energy which dictates the energy cost of rotating the polarization in the system. Along the same lines, the phase-field simulations elucidated that size confinement is the one key parameter for stabilizing such topological structures. Simulations conducted for $(PbTiO_3)_n/(SrTiO_3)_n$ superlattices on $DyScO_3$ (110) substrates[3] revealed that in short-period superlattices ($n < 10$), the ferroelectric phase is stable[3,60] while in large-period superlattices ($n > 25$), the stable structure is a flux-closure pattern,[3,59] but in intermediate-period superlattices ($10 < n < 25$), there is potential for the formation of exotic topological structures such as vortices, skyrmions, or waves as a result of the competition between elastic, electrostatic, and gradient energies.[3,74]

Polar skyrmions

Skyrmions were originally proposed by Skyrme in the 1960s to explain the stability of hadrons as quantized topological defects in three-dimensional (3D) nonlinear sigma models.[75,76] The topological aspects of the skyrmion is characterized by a topological charge as an invariant,

$$Q = \int \left(\frac{\partial \boldsymbol{n}}{\partial x} \times \frac{\partial \boldsymbol{n}}{\partial y} \right) \cdot \boldsymbol{n} d^2 \boldsymbol{r},$$

where $\boldsymbol{n}$ is the unit vector pointing to the magnetization/polarization direction. This topological charge is the in-plane integral of the Pontryagin density.[12]

Further interplay of elastic, electrostatic, and gradient energies in the $(PbTiO_3)_n/(SrTiO_3)_n$ heterostructures provides an intriguing opportunity to produce such complex electric skyrmions (analogous to magnetic skyrmions). Importantly, it was discovered that $(PbTiO_3)_n/(SrTiO_3)_n$ heterostructures have to be grown under a slight compressive strain, for instance, on $SrTiO_3$ (001) substrates, to tip the balance of energies in the right manner to induce these new structures.[2] Looking down at the surface of a $(PbTiO_3)_{16}/(SrTiO_3)_{16}$ superlattice, plan-view STEM images (Fig. 4, middle panel of the top row) reveal long-range ordered arrays of circular features with a size of 8 nm–9 nm, suggesting that this polar order extends through the film over many hundreds of nanometers length scale. Low-resolution, cross-sectional DF-TEM imaging (Fig. 4, blue shaded area in the middle panel of the top row), in turn, revealed a pseudo-long-range periodic array of intensity modulations along both the in- and out-of-plane directions of the superlattice. Atomic-scale polarization mapping using a displacement vector-mapping algorithm was used on both plan-view and cross-sectional high-angle annular dark-field (HAADF)-STEM images to extract the local polarization structures [Figs. 4(a) and 4(b)].[58] The reverse titanium-displacement vector mapping [Fig. 4(a), top] based on the high-resolution plan-view HAADF-STEM image [Fig. 4(a), bottom] reveals a single skyrmion bubble. The reversed titanium displacement is diverging from the edge to the center, corresponding to a hedgehog-like skyrmion structure.[50] To complement this, vector displacement mapping of cross-sectional HAADF-STEM imaging [Fig. 4(b)] clearly shows a cylindrical polar region with anti-parallel (up-down) polarization. The polarization vector rotates at the boundaries near the $PbTiO_3$–$SrTiO_3$ interfaces, consistent with the divergence of polarization observed in plan-view images. The combined plan-view and cross-sectional vector displacement mapping reveals a hedgehog-like structure at the top of the $PbTiO_3$ layer. Along this line, four-dimensional STEM (4D-STEM) with an electron microscope pixel array detector (EMPAD)[77] provides information about the center $PbTiO_3$ layers. In 4D-STEM, the full momentum distribution – that is, the electron diffraction pattern – can be collected at every scan position by the EMPAD. From the diffraction patterns collected on the EMPAD, the reconstructed low-angle annular dark-field (ADF) image [Fig. 4(c)] and the probability current flow in x and y giving the vector components of polar order [Fig. 4(d)] can be obtained. This is largely weighted toward the Bloch-like skyrmion in the middle of the $PbTiO_3$ layer. The combination of hedgehog and Bloch skyrmions is further confirmed by

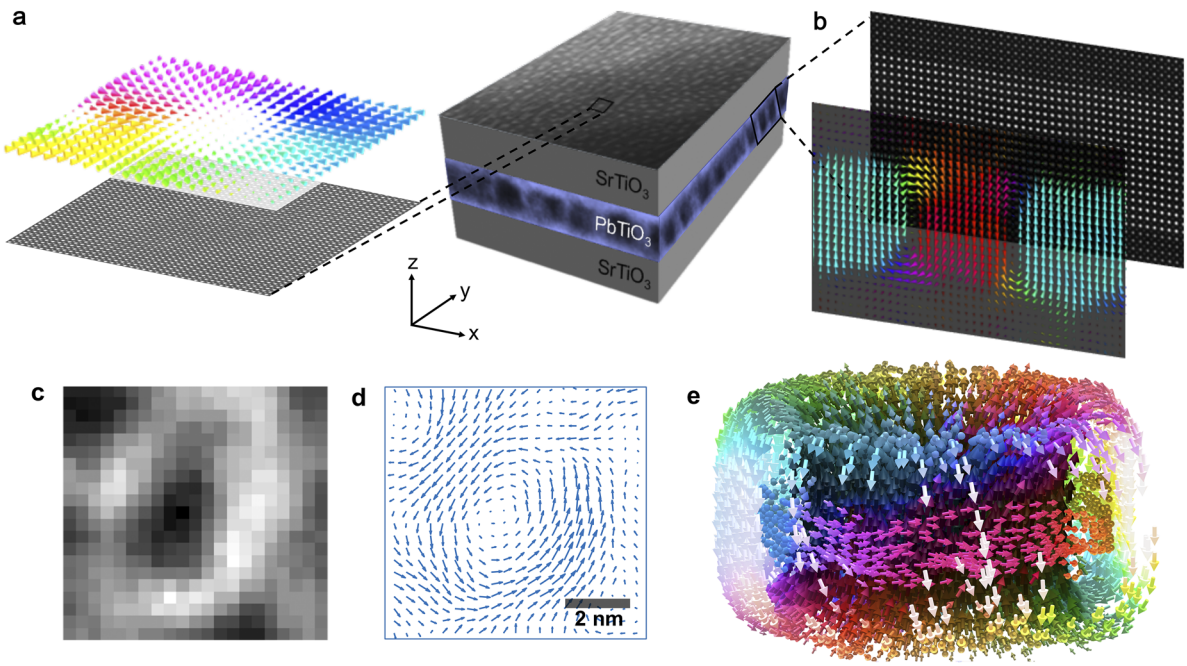

FIG. 4. Long range array of skyrmion structures in $(SrTiO_3)_{16}/(PbTiO_3)_{16}$ superlattice on $SrTiO_3$ (001) substrates. (a) Reversed Ti-ion displacement vector map (top) based on the atomic resolved plan-view HAADF-STEM image (bottom) of a single skyrmion bubble, showing the hedgehog-like skyrmion structure. A cartoon picture of the superlattice (middle of the top panel) is overlaid with the planar view DF-TEM image and shows the 8 nm size circular features all over the samples. (b) Ti displacement vector maps (front) based on the atomic resolved cross-sectional HAADF-STEM image (back), shows a cylindrical domain with anti-parallel (up-down) polarization. The cartoon picture (middle of the top panel) is overlaid with the cross-sectional DF-TEM image and shows the cross-sectional view of the superlattice. The 4D-STEM image of the superlattice gives (c) the annular dark field (ADF) image and (d) maps of polar order using the probability current flow, which were reconstructed from same the 4D data set, where the polarization exhibits a Bloch-like character. (e) Simulation of a single polar skyrmion. Red arrows signify that this is a left-handed skyrmion. The other arrows represent the angular distribution of the dipoles. Reproduced with permission from S. Das, Nature **568**, 368 (2019). Copyright 2019 Springer Nature.

second principles *ab initio* calculations [Fig. 4(e)].[78] This calculation shows the three-dimensional view of a single skyrmion where the polar skyrmions consist of a diverging and converging hedgehog skyrmion pair at the top and bottom, respectively, unlike magnetic skyrmions,[12] and at the center layer, there is a Bloch-type skyrmion structure. The calculated topological charge (Q) is found to be +1 in every case, which reveals that they are topologically equivalent, i.e., one can transform to another by continuous deformation.

PHYSICAL PHENOMENA: CHIRALITY AND NEGATIVE PERMITTIVITY

Chirality of polar skyrmions and vortices

Chirality is a geometrical property that is ubiquitous in nature. When an object is not superimposable on its mirror image, i.e., imparting a handedness or helicity, we call it a "chiral object." Examples include amino acids and sugars in our body and naturally

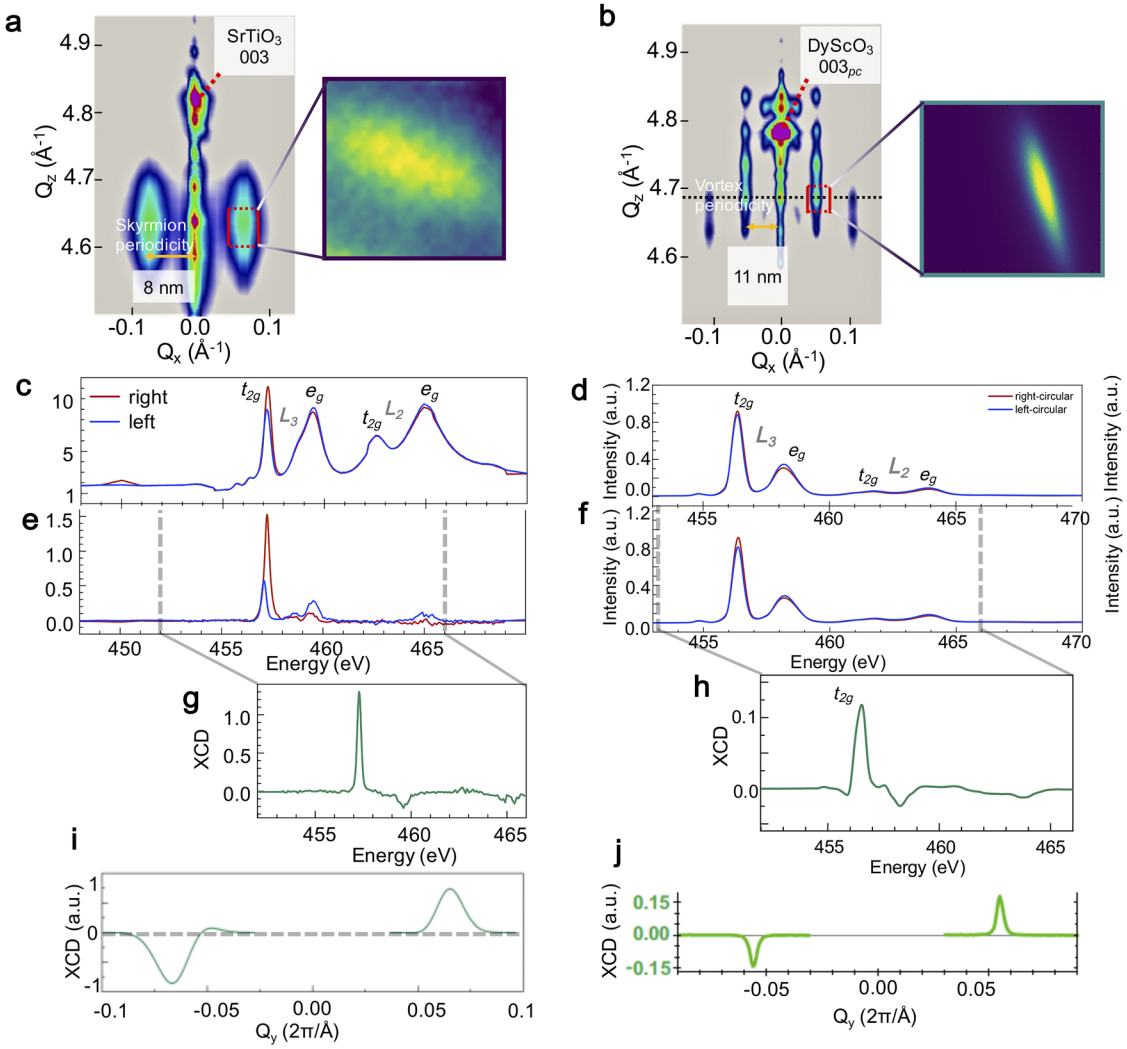

FIG. 5. Resonant soft X-ray diffraction circular dichroism for a $(PbTiO_3)_{16}/(SrTiO_3)_{16}$ superlattice. (a) and (b) Reciprocal space mapping about the (003)-peak of (a) $SrTiO_3$ substrate which contains skyrmion and (b) $DyScO_3$ substrate which contains vortex, shows superlattice peaks running along the Q_z direction, corresponding to the out-of-plane periodicity of about 12 nm, and satellite peaks running along the Q_y direction, corresponding to the in-plane periodicity of about 8 nm for skyrmion and 10 nm for vortex. An image from the CCD used to collect RSXD data, with the resonant diffraction peak clearly visible [right of (a) and (b)]. The satellite peak corresponding to the periodic helical polarization texture that forms within the Bloch skyrmions (a) and the vortex (b) of the central $PbTiO_3$ layers. (c) and (d) Spectra from a satellite peak for right- (red) and left-circularly (blue) polarized light (top panel) for skyrmion (c) and vortex (d), and [(e) and (f)] the same spectra with the background fluorescence subtracted. (g) and (h) The difference spectra (right-circular minus left-circular) (XCD) shows a clear circular dichroism peak at the titanium L_3 t_{2g} edge. (i) and (j) The XCD is measured at a constant energy near resonance as the lateral scattering vector Q_y is varied. The dichroism is always positive for $+Q_y$ and negative for $-Q_y$. The reversal of XCD as the q-vector is inverted is a telltale signature of chirality of the skyrmion (i) and vortex (j). Reproduced with permission from S. Das, Nature **568**, 368 (2019). Copyright 2019 Springer Nature and Shafer *et al.*, Proc. Natl. Acad. Sci. U. S. A. **115**, 915 (2018). Copyright 2018 PNAS.

occurring crystals such as quartz. In the case of $(PbTiO_3)_n/(SrTiO_3)_n$ superlattices, one does not, *a priori*, expect them to be chiral since the constituent layers are by themselves not chiral. When assembled into such superlattices and polar textures begin to form, however, they are found to exhibit chirality. One way to look for chirality in condensed-matter systems is to measure the interaction with circularly polarized electromagnetic radiation, i.e., circular dichroism (XCD).[35] In the case of $(PbTiO_3)_n/(SrTiO_3)_n$ superlattices, recent resonant soft x-ray diffraction studies have shown that the polar vortices in such superlattices do indeed exhibit strong circular dichroism[2,3] (Fig. 5), which is also reminiscent of magnetic-topological structures.[2,35] In hard x-ray reciprocal space mapping (RSM) studies, lateral satellites appear due to the regular spacing of the skyrmions [Fig. 5(a)] and vortex structures [Fig. 5(b)], where the spacing is d_{x_pair} (~8 nm for skyrmions and ~10 nm for vortices). These satellites occur at q-vectors equal to $\pm n \times q_{x\_pair}$, where $q_{x\_pair} = 2\pi/d_{x\_pair}$. By tuning the energy of the x-rays through the titanium $L_{3,2}$ edge (where electronic transitions from the $2p$ to $3d$ levels occur), absorption spectra are collected at q-values corresponding to the satellite peaks. At the titanium $L_{3,2}$ resonance, effects from the electronic structure (specifically the d-orbital configuration) are strongly enhanced. If the spiraling polar distortions that create the skyrmion or vortex phase are chiral, this will manifest as a non-zero circular dichroism since chiral objects interact differently with left- and right-circularly polarized light.[35] By measuring the spectra with both right- and left-circularly polarized light [Figs. 5(c) and 5(d)], subtracting the background fluorescence [Figs. 5(e) and 5(f)], and taking the difference of the two [Figs. 5(g) and 5(h)], circular dichroism (XCD) is indeed observed[2,35] which is strongly indicative of chirality. Furthermore, resonant-scattering intensity is asymmetric with respect to the scattering vector and the sign of the circular dichroism as a function of the lateral scattering vector (Q_y) [Figs. 5(i) and 5(j)].

Negative capacitance state in polar vortices

The phenomenon of negative capacitance has garnered enormous interest due to its exotic physics as well as promise in applications in next-generation electronics[79–82] specifically to overcome the "Boltzmann tyranny" in electronics.[84] Classical Landau–Devonshire–Ginzburg theory of ferroelectrics describes the ferroelectric state through a doubly degenerate free-energy landscape[6] between total free energy G and electric displacement D; the shape of the double-well, free-energy landscape points to the existence of a range of polarizations where the curvature of the free energy (i.e., the second derivative of the free energy with respect to the electric displacement, which is also the permittivity of the material permittivity $\varepsilon \propto \frac{\partial^2 G}{\partial^2 D} < 0$) is negative [hence negative capacitance emerges; Figs. 6(a) and 6(b)]. It should be noted that the entire volume of the material cannot exhibit such a negative permittivity since in that case, it would spontaneously evolve to a state where the curvature of the free energy landscape is positive. Such negative permittivity states can, however, be stabilized in portions of the material or out of equilibrium (i.e., in the temporal regime[83]). A direct measurement of the spatially resolved, steady-state negative capacitance is rare in nature and was first observed microscopically in a vortex structure of $(PbTiO_3)_n/(SrTiO_3)_n$ superlattices.[38] The existence of negative permittivity at the vortex core and the potential-energy landscape across the vortex structure can be directly probed via 4D-STEM.

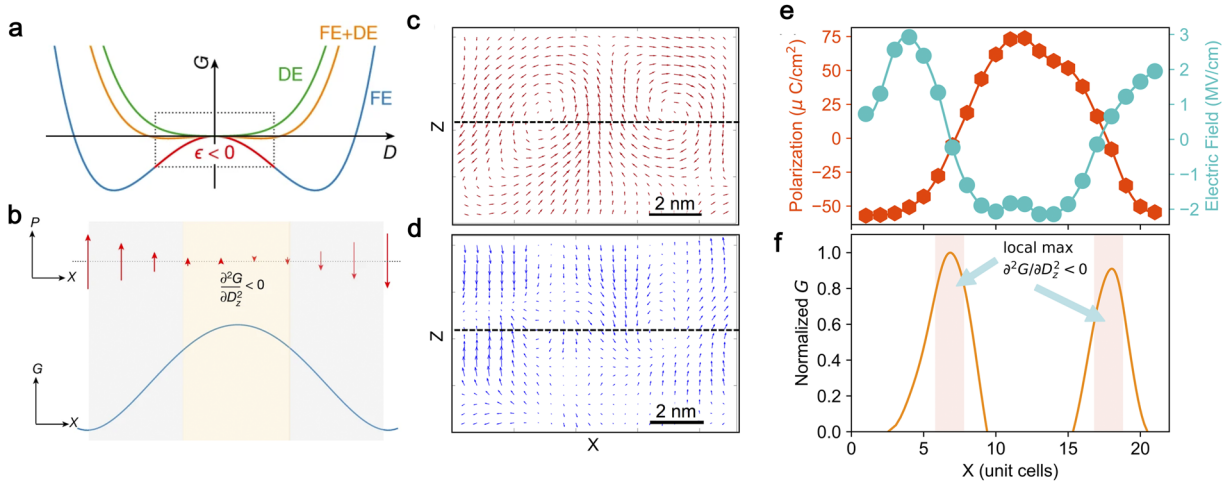

FIG. 6. Measurement of local polarization, electric field and the local double well potential energy of the vortex in a $(SrTiO_3)_{12}/(PbTiO_3)_{12}$ superlattice using EMPAD-STEM. (a) Free energy landscape for a dielectric material (DE), ferroelectric (FE) material and ferroelectric–dielectric (FE–DE) heterostructure. G, free energy; D, displacement. The boundary region (marked by H and K) where the permittivity ε is negative. (b) Spatially resolved energy density (bottom) and the variation in polarization P (top). The polarization is suppressed at the domain walls with maximum energy density than the bulk domain. (c) A cross-sectional polarization vector map of the vortex from a subregion of $PbTiO_3$ layer. (d) Local electric field [corresponding to the same region shown (a)] as measured using TEM. (e) Variation in the z-components of local polarization (*Pz*) and electric field (*Ez*) along a horizontal line [indicated by green dotted line in a and (b)] which passes through the core of vortices. (f), Local energy density estimated from the variation of (*Pz*) and electric field (*Ez*) along the same line. Regions around the core show a negative curvature ($\frac{\partial^2 G}{\partial^2 D} < 0$). Reproduced with permission from Yadav *et al.*, Nature **565**, 468 (2019). Copyright 2019 Springer Nature.

These imaging experiments were carried out in cross-section samples and show the CW-CCW vortex pair [Fig. 6(c)]. The long-range electric fields can be mapped out from the deflection of the electron-beam pattern due to the Lorentz force [Fig. 6(d)].[84] The spatial distribution of polarization (P_z) and electric field (E_z) are measured by focusing along the dashed horizontal line profile [Figs. 6(c)–6(e)], which goes through the vortex core (the magnitude of the measured polarization was calibrated using the polarization of $PbTiO_3$, as shown in Ref. 85). With both the measured electric field and polarization, one can calculate the local potential energy of the system using $dG = EdP$. The estimated potential-energy (G) as a function of P_z across the vortex reveals the existence of a local potential-energy maxima ($\frac{\partial^2 G}{\partial^2 D} < 0$) at the location of the vortex core, where P_z is small [Fig. 6(f)], thus illustrating that the negative capacitance exists in the CW-CCW vortex core.[3] Its intriguing that the existence of such regions of negative capacitance in the material actually leads to an enhancement in the effective dielectric permittivity that can then be probed even by macroscopic measurements.[86] Of greater interest is the fact that such an enhanced dielectric permittivity can be significantly changed with an electric field. This occurs through the destruction of the vortex/skyrmion state under the electric field, and the superlattice converts into a "normal" ferroelectric layer, thus representing a topological phase transition accompanied by a change in the topological charge from a finite value to zero at a finite field. Removal of the electric field restores the skyrmionic state.

SUMMARY AND OUTLOOK

The chiral-polar topologies and their associated complex phase mixtures suggest the presence of exotic physical responses in these ferroelectric superlattices. Along with gaining fundamental knowledge about them, researching and understanding vortices and skyrmions can lead to new technological applications, particularly those that take advantage of the negative capacitance that is embedded in the vortices/skyrmions. Specially, they could be used in skyrmionics – a new type of memory storage where data are encoded using the chirality of the individual skyrmion.[18,19] Magnetic skyrmions can be controlled by utilizing cross coupling between magnetic and electrical parameters, e.g., switching and controlling of chirality using electric or magnetic fields. The use of electric fields is preferable for reducing the power consumption associated with the switching. The control of chirality with the use of homogeneous dc fields can be achieved with skyrmions and/or vortices, which can couple to homogeneous electric/magnetic fields, and an electrically switchable chirality could be realized. In addition, the chiral domain walls with different handedness in solid-state ferroelectric materials have never been observed. In a confined ferroelectric, it would be interesting to demonstrate the polar vortex domains with anti-phase boundaries as three-dimensional (3D) polarization textures which exhibit collective behavior, in the form of chiral domain walls. The prospect for control of chirality in both magnetic systems and polar skyrmions/vortices depends on the ability to easily switch their handedness, which will require coupling to a homogeneous electric field.[87–89] The ability to switch chirality with homogeneous magnetic fields[35] or ac electric currents[93] has been demonstrated for magnetic structures, and switching by electric fields is possible with, for example, the imposition of voltage-induced strain.[12] In polar skyrmion/vortex structures, their chiral nature[2,35] and toroidal coupling to electric fields[45] have already been established, and attempts to utilize this coupling to achieve electric-field control of chirality are underway. So far, studies demonstrate chirality switching in magnetic structures on the scale of hundreds of nanometers. Although theoretical predictions show that switching can occur in sub-100-nm electric and magnetic nanostructures,[60,63] these are difficult to realize experimentally. Thus, a significant challenge in the coming years will be the development of methods to write and read chirality on the nanoscale in such a way that it is useful for devices. The glassy behavior and extremely "soft" nature of the polarization and frequency dispersion pointing toward macroscale collective response of the vortices have been predicted in $PbTiO_3/SrTiO_3$ heterostructures. In addition, strain-based routes to produce samples exhibiting a 100% vortex phase or polar skyrmion features are being explored; these can be used as model systems for in-depth studies of the physics and nature of these complex phases.[90] Imaging chiral domain walls at the nanoscale is possible with *in situ* techniques such as spin-polarized low energy electron microscopy (SPLEEM)[91] and x-ray magnetic circular dichroism microscopy (XMCD),[92] and chiral domain walls in ferroelectrics have been demonstrated using second-harmonic generation microscopy.[93] Moving forward, these or related techniques may inspire new mechanisms through which the deterministic writing and reading of nanoscale chiral structures can be achieved. In addition, electric field manipulation of spins has attracted interest due to their promise for new functionalities and low power device concepts. Using a dilute Fe-doped ferroelectric $PbTiO_3/SrTiO_3$ as a model system, one can demonstrate electric field manipulation of spin directionality in individual spins. The intriguing potential for coupled effects between spin and polarization could also lead to new modalities of data storage. The topological phase transition and the production of steady-state negative capacitance and large field-tunable response of these emergent states could promise for electronic applications.

ACKNOWLEDGMENTS

This work was supported by the Quantum Materials Program from the Office of Basic Energy Sciences, U.S. Department of Energy (Grant No. DE-AC02-05CH11231). L.W.M. acknowledges support from the U.S. Department of Energy, Office of Science, Office of Basic Energy Sciences, under Award No. DE-SC-0012375, for the development and study of ferroic heterostructures.

DATA AVAILABILITY

The data that support the findings of this study are available within the article or from the corresponding author upon reasonable request.

REFERENCES

[1] U. K. Rößler, A. N. Bogdanov, and C. Pfleiderer, Nature **442**, 797 (2006).
[2] S. Das, Nature **568**, 368 (2019).
[3] A. K. Yadav *et al.*, Nature **530**, 198 (2016).
[4] V. A. Stoica *et al.*, Nat. Mater. **18**, 377 (2019).
[5] J. Valasek *et al.*, Phys. Rev. **17**, 475 (1921).
[6] M. E. Lines and A. M. Glass, *Principles and Applications of Ferroelectrics and Related Materials* (Oxford Scholarship, 2010).

[7]R. Ramesh and D. G. Schlom, Nat. Rev. Mat. **4**, 257 (2019).
[8]J. C. Wojdeł, P. Hermet, M. P. Ljungberg, P. Ghosez, and J. Íñiguez, J. Phys.: Condens. Matter **25**, 305401 (2013).
[9]Q. Li *et al.*, J. Synchrotron Radiat. **26**, 1790 (2019).
[10]S. Manipatruni *et al.*, Nature **565**, 35–42 (2019).
[11]J. Seidel, R. K. Vasudevan, and N. Valanoor, Adv. Electron. Mater. **2**, 1500292 (2016).
[12]N. D. Mermin, Rev. Mod. Phys. **51**, 591 (1979).
[13]F. D. M. Haldane, Rev. Mod. Phys. **89**, 040502 (2017).
[14]J. M. Kosterlitz, Rev. Mod. Phys. **89**, 040501 (2017).
[15]Y. Ohuchi, J. Matsuno, N. Ogawa, Y. Kozuka, M. Uchida, Y. Tokura, and M. Kawasaki, Nat. Commun. **9**, 213 (2018).
[16]L. Wang, Q. Feng, Y. Kim, R. Kim, K. H. Lee, S. D. Pollard, Y. J. Shin, H. Zhou, W. Peng, D. Lee, W. Meng, H. Yang, J. H. Han, M. Kim, Q. Lu, and T. W. Noh, Nat. Mater. **17**, 1087 (2018).
[17]X.-L. Qi and S.-C. Zhang, Rev. Mod. Phys. **83**, 1057 (2011).
[18]S. S. P. Parkin, M. Hayashi, and L. Thomas, Science **320**, 190 (2008).
[19]A. Fert, V. Cros, and J. Sampaio, Nat. Nanotechnol. **8**, 152 (2013).
[20]R. Tomasello, E. Martinez, R. Zivieri, L. Torres, M. Carpentieri, and G. Finocchio, Sci. Rep. **4**, 6784 (2015).
[21]X.-K. Wei, C.-L. Jia, T. Sluka, B.-X. Wang, Z.-G. Ye, and N. Setter, Nat. Commun. **7**, 12385 (2016).
[22]S. Cherifi-Hertel, H. Bulou, R. Hertel, G. Taupier, K. D. H. Dorkenoo, C. Andreas, J. Guyonnet, I. Gaponenko, K. Gallo, and P. Paruch, Nat. Commun. **8**, 15768 (2017).
[23]G. De Luca, M. D. Rossell, J. Schaab, N. Viart, M. Fiebig, and M. Trassin, Adv. Mater. **29**, 1605145 (2017).
[24]J. Seidel *et al.*, Nat. Mater. **8**, 229–234 (2009).
[25]J. Guyonnet, I. Gaponenko, S. Gariglio, and P. Paruch, Adv. Mater. **23**, 5377–5382 (2011).
[26]P. Maksymovych *et al.*, Nano Lett. **11**, 1906–1912 (2011).
[27]M. Daraktchiev, G. Catalan, and J. F. Scott, Phys. Rev. B **81**, 224118 (2010).
[28]S. Y. Yang *et al.*, Nat. Nanotechnol. **5**, 143–147 (2010).
[29]N. Nagaosa and Y. Tokura, Nat. Nanotechnol. **8**, 899 (2013).
[30]J. M. Gregg, Ferroelectrics **433**, 74 (2012).
[31]N. Strkalj *et al.*, Materials **12**, 3108 (2019).
[32]S. Das, A. Ghosh, M. R. McCarter, S.-L. Hsu, Y.-L. Tang, A. R. Damodaran, R. Ramesh, and L. W. Martin, APL Mater. **6**, 100901 (2018).
[33]G. Tian, W. Yang, D. Chen, Z. Fan, Z. Hou, M. Alexe, and X. Gao, Natl. Sci. Rev. **6**, 684 (2019).
[34]S. Chen *et al.*, Adv. Mater. 2020, 2000857.
[35]P. Shafer *et al.*, Proc. Natl. Acad. Sci. U. S. A. **115**, 915 (2018).
[36]M. Mochizuki *et al.*, Nat. Mater. **13**, 241–246 (2014).
[37]B. Li *et al.*, RSC Adv. **3**, 7928–7932 (2013).
[38]A. K. Yadav *et al.*, Nature **565**, 468 (2019).
[39]C. Kittel, Rev. Mod. Phys. **21**, 541 (1949).
[40]C. Kittel, Phys. Rev. **70**, 965, 97l (1946).
[41]R. Pulwey, M. Zölfl, G. Bayreuther, and D. Weiss, J. Appl. Phys. **91**, 7995 (2002).
[42]P.-O. Jubert, J.-C. Toussaint, O. Fruchart, C. Meyer, and Y. Samson, Europhys. Lett. **63**, 132 (2003).
[43]R. Hertel, O. Fruchart, S. Cherifi, P.-O. Jubert, S. Heun, A. Locatelli, and J. Kirschner, Phys. Rev. B **72**, 214409 (2005).
[44]T. Shinjo, T. Okuno, R. Hassdorf, K. Shigeto, and T. Ono, Science **289**, 930 (2000).
[45]J. Park, P. Eames, D. Engebretson, J. Berezovsky, and P. Crowell, Phys. Rev. B **67**, 020403 (2003).
[46]T. Nagai, H. Yamada, M. Konoto, T. Arima, M. Kawasaki, K. Kimoto, Y. Matsui, and Y. Tokura, Phys. Rev. B **78**, 180414 (2008).
[47]R. K. Vasudevan *et al.*, ACS Nano **5**, 879–887 (2011).
[48]S. Mühlbauer, B. Binz, F. Jonietz, C. Pfleiderer, A. Rosch, A. Neubauer, R. Georgii, and P. Böni, Science **323**, 915 (2009).
[49]X. Z. Yu, Y. Onose, N. Kanazawa, J. H. Park, J. H. Han, Y. Matsui, N. Nagaosa, and Y. Tokura, Nature **465**, 901 (2010).
[50]K. Runge, Y. Nozaki, Y. Otani, H. Miyajima, B. Pannetier, T. Matsuda, and A. Tonomura, J. Appl. Phys. **79**, 5075 (1996).
[51]J. Cho *et al.*, Nat. Commun. **6**, 7635 (2015).
[52]I. I. Naumov, L. Bellaiche, and H. Fu, Nature **432**, 737–740 (2004).
[53]H. Fu and L. Bellaiche, Phys. Rev. Lett. **91**, 257601 (2003).
[54]L. Lu *et al.*, Phys. Rev. Lett. **120**, 177601 (2018).
[55]Z. Wu *et al.*, Phys. Rev. B **68**, 014112 (2003).
[56]P. Sharma *et al.*, Materials **12**, 2927 (2019).
[57]E. A. Eliseev *et al.*, J. Appl. Phys. **106**, 084102 (2009).
[58]C.-L. Jia, K. W. Urban, M. Alexe, D. Hesse, and I. Vrejoiu, Science **331**, 1420–1423 (2011).
[59]C. T. Nelson *et al.*, Nano Lett. **11**, 828–834 (2011).
[60]Y. L. Tang *et al.*, Science **348**, 547–551 (2015).
[61]P. Noël *et al.*, Nature **580**, 483–486 (2020).
[62]E. Bousquet, M. Dawber, N. Stucki, C. Lichtensteiger, P. Hermet, S. Gariglio, J.-M. Triscone, and P. Ghosez, Nature **452**, 732 (2008).
[63]D. Sichuga *et al.*, Phys. Rev. Lett. **104**, 207603 (2010).
[64]J. H. Zhao *et al.*, Phys. Rev. B **89**, 174101(R) (2014).
[65]P. Zubko, J. C. Wojdeł, M. Hadjimichael, S. Fernandez-Pena, A. Sené, I. Luk'yanchuk, J.-M. Triscone, and J. Íñiguez, Nature **534**, 524 (2016).
[66]S. Salahuddin and S. Datta, Nano Lett. **8**, 405–410 (2008).
[67]N. Choudhury, L. Walizer, S. Lisenkov, and L. Bellaiche, Nature **470**, 513 (2011).
[68]S. Prosandeev and L. Bellaiche, Phys. Rev. B **75**, 094102 (2007).
[69]S. Prosandeev *et al.*, J. Phys. Condens. Matter **20**, 193201 (2008).
[70]Zhang *et al.*, Adv. Mater. **29**, 1702375 (2017).
[71]Zhang *et al.*, Advanced Functional Materials **29**, 1808573 (2019).
[72]Y. Qi *et al.*, J. Appl. Phys. **111**, 104117 (2012).
[73]J. J. Wang, X. Q. Ma, Q. Li, J. Britson, and L.-Q. Chen, Acta Mater. **61**, 7591–7603 (2013).
[74]A. R. Damodaran *et al.*, Nat. Mater. **16**, 1003 (2017).
[75]T. H. R. Skyrme, Proc. R. Soc. A **247**, 260–278 (1958).
[76]T. H. R. Skyrme, Proc. R. Soc. A **252**, 236–245 (1959).
[77]M. W. Tate *et al.*, Microsc. Microanal. **22**, 237–249 (2016).
[78]P. García-Fernández, J. C. Wojdeł, J. Íñiguez, and J. Junquera, Phys. Rev. B **93**, 195137 (2016).
[79]S. Salahuddin and S. Datta, in *IEEE International Electron Devices Meeting* (IEEE, 2008), pp. 1–4.
[80]A. I. Khan, D. Bhowmik, P. Yu, S. J. Kim, X. Pan, R. Ramesh, and S. Salahuddin, Appl. Phys. Lett. **99**, 113501 (2011).
[81]T. N. Theis and P. M. Solomon, Science **327**, 1600 (2010).
[82]M. Si *et al.*, Nature Nanotechnology **13**, 24 (2018).
[83]A. I. Khan *et al.*, Nat. Mater. **14**, 182 (2015).
[84]C. Kittel, *Introduction to Solid State Physics* (Wiley, Hoboken, 1966).
[85]Y. Watanabe, in *Ferroelectric Thin Films: Basic Properties and Device Physics for Memory Applications*, edited by M. Okuyama and Y. Ishibashi (Springer, Berlin, 2005), Vol. 177-199.
[86]S. Das *et al.*, "Local negative permittivity and topological phase transition in polar skyrmions," Nat. Mater. (published online, 2020).
[87]M. Jaafar, R. Yanes, D. Perez de Lara, O. Chubykalo-Fesenko, A. Asenjo, E. M. Gonzalez, J. V. Anguita, M. Vasquez, and J. L. Vicent, Phys. Rev. B **81**, 054439 (2010).
[88]K. Yamada, S. Kasai, Y. Nakatani, K. Kobayashi, H. Kohno, A. Thiaville, and T. Ono, Nat. Mater. **6**, 270 (2007).
[89]R. P. Beardsley, S. Bowe, D. E. Parkes, C. Reardon, K. W. Edmonds, B. L. Gallagher, S. A. Cavill, and A. W. Rushforth, Sci. Rep. **7**, 7613 (2017).
[90]Z. Hong *et al.*, Nano Lett. **17**, 2246–2252 (2017).
[91]J. P. Titene *et al.*, Nat. Commun. **6**, 6733 (2015).
[92]F. P. Chmiel *et al.*, Nat. Mater. **17**, 581–585 (2018).
[93]T. Kämpfe, P. Reichenbach, M. Schröder, A. Haußmann, L. M. Eng, T. Woike, and E. Soergel, Phys. Rev. B **89**, 035314 (2014).